INVITED PAPER 3942
SPIE Optics East 23-26 October 2005, Boston USA

Microstructured fibres for sensing applications

M.N. Petrovich[a]*, A. van Brakel[a], F. Poletti[a], K. Mukasa[a,c], E. Austin[a], V. Finazzi[a], P. Petropoulos[a], E. O'Driscoll[d], M. Watson[d], T. DelMonte[d], T.M. Monro[b], J.P. Dakin[a], D.J. Richardson[a]

[a]Optoelectronics Research Centre (ORC), University of Southampton; Southampton, UK
[b]Now at the School of Chemistry and Physics, University of Adelaide; Adelaide, SA, Australia.
[c]On leave from Furukawa Electric Co. Ltd. Fitel-Photonics Laboratory, Ichihara, Chiba, Japan
[d]BAE SYSTEMS Advanced Technology Centre, Sowerby Building, Bristol, UK

ABSTRACT

Microstructured fibres (MOFs) are among the most innovative developments in optical fibre technology in recent years. These fibres contain arrays of tiny air holes that run along their length and define the waveguiding properties. Optical confinement and guidance in MOFs can be obtained either through modified total internal reflection, or photonic bandgap effects; correspondingly, they are classified into index-guiding Holey Fibres (HFs) and Photonic Bandgap Fibres (PBGFs). MOFs offer great flexibility in terms of fibre design and, by virtue of the large refractive index contrast between glass/air and the possibility to make wavelength-scale features, offer a range of unique properties. In this paper we review the current status of air/silica MOF design and fabrication and discuss the attractions of this technology within the field of sensors, including prospects for further development. We focus on two primary areas, which we believe to be of particular significance. Firstly, we discuss the use of fibres offering large evanescent fields, or, alternatively, guidance in an air core, to provide long interaction lengths for detection of trace chemicals in gas or liquid samples; an improved fibre design is presented and prospects for practical implementation in sensor systems are also analysed. Secondly, we discuss the application of photonic bandgap fibre technology for obtaining fibres operating beyond silica's transparency window, and in particular in the 3μm wavelength region.

Keywords: Microstructured, holey, photonic crystal, band-gap, fibre, mid-infrared, fibre sensing.

1. INTRODUCTION

Microstructured Optical Fibres (MOFs) have developed into a topic of intense scientific interest over the past few years[1-5]. These fibres have wavelength-scale features with high index contrast in their transverse cross section, which define the optical waveguide and provide a range of unusual properties. In the most common type of MOFs, the regions of high index contrast are provided by fine arrays of air holes that extend along the full fibre length. The vast majority of air/silica microstructured fibres reported to date are fabricated either from undoped silica[1,3,5] or compound glasses (including chalcogenide[6], lead silicate[7], tellurite[8] and bismuth silicate[9]); however MOFs made of polymers[10] and polycrystalline materials[11] have also been reported. The single most important characteristic of MOFs is that the mode propagation properties are strongly dependent on the wavelength and can be tailored through careful design of the configuration and geometry of the air holes. Since the latter can be specified with a wide degree of freedom (for instance by controlling the number, size, shape, and arrangement of the air holes), a substantially broader range of interesting and technologically enabling properties can be achieved in MOFs, than in the more conventional fibres based on a solid cladding and a doped glass core. These include, amongst others, broad-band single mode guidance, unique and tailorable dispersion properties, extremely high (or extremely low) nonlinearities and guidance in an air core.

A common way to classify microstructured fibres is based on the mechanism by which light guidance is achieved. *Holey Fibres* (HFs) possess a solid core surrounded by a cladding region laced with air holes, which act as index-decreasing elements. Light is guided by virtue of a modified form of total internal reflection, since the refractive index of the core is

* Email: mnp@orc.soton.ac.uk, phone: +44 (0) 2380593836, fax: +44 (0) 230593149, http:// www.orc.soton.ac.uk

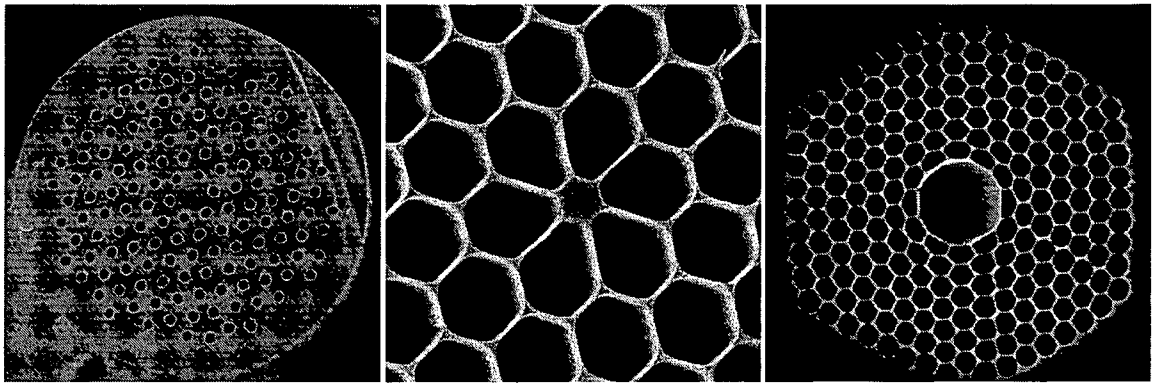

Figure 1: Some typical air-silica microstructured fibres: (a) Large Mode Area Holey Fiber (LMA-HF), (b) Small mode area, Highly-Nonlinear Holey Fiber (HNL-HF), (c) Air-guiding photonic bandgap fiber (PBGF).

greater than the effective index of the surrounding cladding region (figure 1a-b). Although a periodic structure is not required in order to obtain guidance by average index effect[12], HFs often exhibit a periodic cladding structure due to the fabrication processes used, thus they are frequently known as *Photonic Crystal Fibers* (PCFs). A periodic arrangement of holes is, on the other hand, essential for light confinement in the second class of MOFs - referred to as *Photonic Bandgap Fibers* (PBGFs)[13] (figure 1c). In PBGFs, light within certain wavebands is prevented from propagating in the cladding region due to bandgap effects. The core is formed by introducing a low index defect; photonic bandgap fibers are able to support guidance in air[13].

Optical fibers are well established for sensing applications, and have been particularly successful in the areas of distributed sensing[14,15,16], fiber Bragg grating sensors[17,18], fiber gyroscopes[18,19] and acoustic sensors[20]. Fiber-based sensors have some important advantages over competing technologies, such as immunity to electromagnetic interference, low weight, small size, high sensitivity and large bandwidth. The advent of microstructured fibers has opened up several new opportunities in this field. A first application area of MOFs is chemical sensing, where the guided light is used to sample liquid or gas specimens contained in the holes[21]. HFs can be designed to have a significant fraction of the optical field propagating in the holes surrounding the core[22], while, in air-guiding PBGFs, as much as 99% of the optical field is located in the hollow core, allowing for an extremely efficient interaction with samples contained in it. Another application area arises from the strong dependence of the propagation properties of MOFs on the geometry of the holey region. The latter is inherently sensitive to external factors, such as temperature and strain[23], bending[24] or hydrostatic pressure[25], and the cladding geometry can be tailored to achieve a better response than in standard fibers.

MOFs have also been investigated as components for use in optical sensors. For instance, high-nonlinearity, dispersion-tailored MOFs can be used for generation of high-brightness, ultra-broadband novel light sources covering regions of the spectrum otherwise difficult to access using conventional sources[26]. Such sources have found application in spectroscopy and high resolution tomography[27]. Furthermore, MOFs offer clear advantages for power delivery in remote sensing applications, where MOFs may outperform conventional fibers in some cases. For instance, large mode area (LMA) Holey Fibers and PBGFs offer advantages for the delivery of high-energy diffraction-limited beams due to reduced nonlinear and damage thresholds. Photonic bandgap fibers can be designed to operate at mid-IR[28] wavelengths, which are completely outside the operational range of conventional fibers (due to the high material loss of silica) and have great relevance for remote and chemical sensing.

2. FABRICATION AND PROPERTIES OF MICROSTRUCTURED FIBRES

2.1. Index-guiding Holey Fibres

Air/silica microstructured fibres are generally fabricated using a *stack-and-draw* technique. High-purity, low-OH silica rods and capillary tubes of appropriate size and aspect ratio are prepared and individually positioned to form the

required structure. The most common arrangement is a close-packed triangular geometry, although different lattices can be obtained by using more complex arrangements of rods and capillaries[29], or different types of doped silica[30]. The core is obtained by replacing one or more hollow capillaries at the centre of the array with solid rods. A *preform*, which contains the required structure on a ≈mm scale, is ultimately obtained by inserting the stacked array into a jacketing tube. The preform is then drawn to fibre size in a conventional fibre drawing tower. This can either be accomplished in a single step, or, if a large scale-reduction factor is required, a two step procedure can also be employed. In the latter case, the microstructured preform is first drawn into a cane, which is then over-clad by a solid silica jacket and finally drawn to fibre. This procedure allows extremely small features to be obtained whilst retaining good mechanical properties. Positive and/or negative pressure differentials can be applied to different regions of the preform during the draw in order to maintain its geometry and help counteract the effect of surface tension at the drawing temperature. The structure of the final fibre is primarily defined through the lattice geometry and two critical design parameters: the *hole-to-hole spacing*, Λ, and the *relative hole size*, d/Λ (d being the *hole diameter*). Note that, if the holes have a round shape, the d/Λ ratio also characterises the *air filling factor* (AFF), i.e. the total percentage of void regions in the transverse cross section of the fibre. For fibres with very high AFFs, the holes tend to become hexagonally distorted (Fig. 1b); thus, the actual value of AFF in the drawn fibre depends on the degree of distortion (this is generally described by the radii of curvature at the nodal points[31]).

The stack-and-draw method offers considerable flexibility in choosing the individual elements and designing the properties of the core and cladding regions. For instance, large mode area (LMA) and small, highly nonlinear (HNL) single mode fibres, high-NA, double-clad and multicore fibres, as well as fibres doped with rare earths or photosensitive ions can be fabricated using this method[32]. The multiple steps and material handling that are required in the fabrication of stacked performs has required the development of suitable procedures to eliminate contaminants (most notably surface OH). As a result of such efforts and more general developments in fabrication and design, microstructured fibre technology has now reached a level where multi-kilometer lengths of polymer coated air/silica fibres with losses as low as 0.28dB/km at 1.55μm[33] can be reliably fabricated.

It is important to note that microstructured performs have also been obtained via other techniques, including drilling[34], extrusion[35] and built-in casting of sol gels[36]. Although these methods are generally less flexible than the stack-and-draw technique, and the resulting fibres generally exhibit higher losses, they might hold some merit in the case of less complicated structures because they are less labour-intensive and more cost-effective then stack-and-draw when the base material is not readily available in large volumes. Extrusion, in particular has been demonstrated to be an extremely convenient technique for producing small core fibres with very large air filling factors[26,35] using materials with low melting points, such as soft glasses and polymers. Notice also that index-guiding fibres do not require that their holes are arranged in a regular lattice. Random-hole holey fibres have been fabricated by stacking[37], however an interesting alternative procedure has recently emerged[38]. Here, a holey cladding is obtained by introducing a gas-producing chemical formulation in the preform. Elongated air holes are then produced *in situ* by allowing the gas bubbles to be stretched as the fibre is drawn.

2.1.1. Photonic Bandgap Fibres

Photonic bandgap fibres (PBGFs) operate by means of a fundamentally different light guiding mechanism to that of conventional fibres[39]. Rather than relying on modified total internal reflection, PBGFs exploit bandgap effects[40] arising from the highly regular array of air holes that form the cladding region. Here, propagation in the transverse plane is prohibited at well-defined optical frequencies. By suitably breaking the symmetry of the cladding, for instance introducing an oversized air hole, a "defect" is created where a localized optical mode can exist. Such a defect acts as the core, guiding light within the frequency windows defined by the surrounding 2-D photonic crystal cladding. In contrast to index guiding fibres, the core of PBGFs is not required to have a higher refractive index than the cladding and thus propagation can take place in an air core. In the case of air/silica PBGF, it has been demonstrated[41] that low-loss air guidance at visible and near-infrared wavelengths can be obtained in structures based on a triangular lattice with small hole-to-hole spacing ($\Lambda \approx 1.8\text{-}2.2\lambda$) and with very large air filling factors (AFF≈75% or higher)[42]. An example of the type of PBGF considered here is shown in figure 1c. In this particular case, the core is obtained by the omission of seven elements from the centre of the stack; fibres with larger cores can be obtained by omitting more elements. The hollow core region is surrounded by seven to eight complete rings of holes.

Photonic bandgap fibres are produced by the same stack-and-draw technique that was previously described for holey fibres[43]; the fabrication of PBGFs, however, is more challenging than their index guiding MOF counterparts due to the requirement of high AFF and small Λ. Crucially, since guidance relies upon resonant scattering from a regular 2-D lattice, PBGFs are extremely sensitive to structural imperfections. In addition, the transmission properties of PBGFs are critically dependent on the structural parameters of the photonic crystal cladding. For instance, small changes of the hole-to-hole spacing or air filling factor produce substantial differences in the position and width of the bandgaps. Consequently, the transmission of PBGFs is also very sensitive to structural variations along their length. Finally, unoptimised configurations of the core boundary lead to the existence of surface modes[44], which may introduce extra loss at wavelengths within the bandgap.

Despite the difficulties, fabrication of PBGFs has matured at an impressive rate in the last few years; typical losses were lowered from ≈1000dB/km to ≈1dB/km[45] in just over three years, and kilometer lengths of high quality PBGFs can now be reliably fabricated. Apart from the sensing applications, which are the focus of this paper, there is strong interest in PBGFs for power delivery[46], high-energy pulse manipulation[47], spectroscopy[48] and particle propulsion[49]. Furthermore, because the mode overlap with the solid structure can be as low as a few percent and, given that most gases (including air) have intrinsically lower values of optical attenuation and much wider transmission than silica glass, hollow core silica PBGFs offer the tantalizing prospect of transmission beyond silica's own transparency window. For instance, transmission could be possible at mid-infrared wavelengths, which is of course extremely attractive for a range of applications including optical sensing.

Bragg fibres are a different class of photonic bandgap fibres[50]. Here the fibre cladding is composed of concentric cylindrical layers of high and low refractive index materials, which act as a Bragg reflector for certain wavebands. These fibres were first demonstrated using alternating layers of a polymer and a chalcogenide material[28], which provided extremely high refractive index contrast and allowed light guidance in an air core. More recently, air/silica Bragg fibres have also been reported[51], in which the regions of high contrast are obtained by introducing concentric rings of expanded air holes surrounding a hollow core.

3. DESIGN AND FABRICATION OF INDEX-GUIDING HOLEY FIBRES FOR EFFICIENT EVANESCENT-WAVE SENSORS

3.1. Evanescent wave sensing using MOFs

The presence of arrays of air columns in microstructured fibres provides an ideal platform for the indiffusion of gas-phase and liquid-phase formulations, and their close proximity to the guided optical mode makes MOFs suitable for absorption-based sensor devices[52]. Here, the concentration of chemicals is determined by measuring the absorption that occurs for specific wavelengths as light propagates through a sample. Optical fibre devices based on conventional fibres have found limited application for chemical sensing due to the small mode field overlap and/or high loss[53]. In contrast, HFs can be designed in such a way that a consistent fraction of the optical field propagates in the holes surrounding the core[52]. Better still, in air-guiding PBGFs as much as 99% of the optical field is typically located in air, allowing extremely efficient interaction if a material is directly placed in the core. With transmission losses now down to the dB/km level, MOFs can provide long interaction lengths (hence high sensitivity) in a compact fashion, thus offering a substantial improvement as compared to systems based on bulk cells and unguided beams of light. This is attractive e.g. for detection of trace chemicals or biomolecules. Extremely small volumes (≈μl per meter length) are required to fill the holes of MOFs, which is highly desirable when sampling hazardous substances or expensive preparations.

The use of PBGFs for gas sensing will be discussed in section 4. Here we concentrate on the design and fabrication of index-guiding holey fibres with very high mode field overlap for use as evanescent field sensors. Holey fibres were the first type of MOF originally proposed for chemical sensing[54]. In this type of MOF, the optical mode is primarily confined to the solid core. However, a fraction of the optical field propagates within the holes located in close proximity to the core, thus allowing for interaction with specimens through evanescent field effects. Early design studies[54] pointed out that careful design of the fibre geometry can afford reasonably high overlap between the guided light and the air holes. It was shown that a higher mode penetration into the holes surrounding the core correlates with a smaller hole-to-hole spacing, Λ, and with higher values of d/Λ, i.e. of air filling factor. Indeed, the strength of the evanescent field (at a

fixed wavelength λ) increases on decreasing core size in HFs. When the latter is comparable to λ, a large fraction of the optical field propagates in the hollow region as an evanescent field[54]. Most HFs are based on a triangular lattice of holes, with the central hole replaced by a rod and where the size of the resulting core is generally comparable to the lattice spacing Λ. Ref. 54 proposes the following rule of thumb, valid for fibres with high air filling factors: $\lambda \geq 2.2\Lambda$ and shows that structures with up to 30% of power in air at 1.55 μm are feasible if such condition is satisfied. The confinement loss, however, also increases by increasing λ/Λ, although it can be reduced by adding more rings of holes. Structures with small pitch, high air filling factor and a large number of elements are generally difficult to obtain, thus fabrication ultimately poses a limit on the maximum overlap that is achievable in this type of structure. Hoo et al.[55,56] have studied the sensor performance of commercially available HNL-HFs and found a maximum overlap factor of 12.6% at 1.53μm[57]. While this represented a very substantial improvement compared to any previous fibre-based evanescent sensor[53], it is still less than expected from theoretical predictions. Here we describe a new and substantially improved index-guiding HF structure which has the potential to provide very high mode field overlap.

3.2. Fabrication of a very holey fibre structure with high air-mode overlap

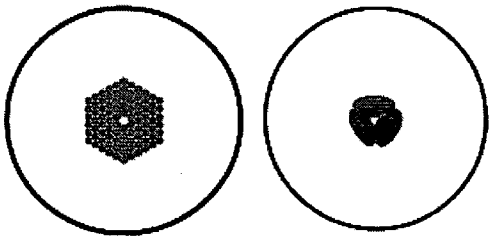

Figure 2: Two different types of index-guiding Holey Fibre: the conventional, centre-hole omitted type (left) and the suspended core type considered in this study.

In this study, we propose a different type of index guiding structure that can achieve significantly higher mode overlap than previously reported, without the limitations discussed in the previous section. The basic idea is shown in figure 2: the hollow region is composed of just three holes, and the core is suspended on thin struts; we term this structure *suspended core* holey fibre (SC-HF). A similar structure has been obtained previously in soft glass using an extrusion technique[7,9]. The simple structure of SC-HFs presents some key advantages over regular lattice-based structures. Firstly, the fabrication of the preform is considerably less labour-intensive. Secondly, the core size can be chosen to be very small, and the holes can be made much larger than the core dimensions. The confinement loss, as will be shown later, can be made very small, by allowing the struts to be sufficiently long and thin.

We employed high precision ultrasonic drilling to fabricate the microstructured preform (figure 4a). The latter was drawn into a fibre via a two-step process, where the three holes were expanded to the required size. Several fibres with different core dimensions were fabricated. The one shown in figure 3 has ≈0.8μm core diameter, the cladding holes

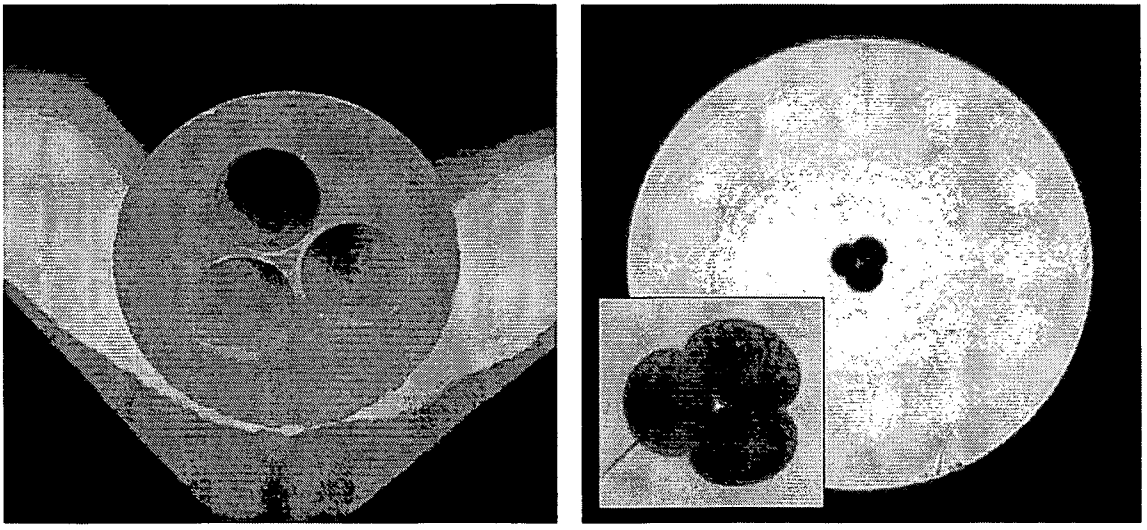

Figure 3: Fabrication of a suspended core (SC) Holey Fibre: drilled preform (left); final drawn fibre (right)

measure ≈11μm in the radial direction and the struts are approximately 8μm long in their thinnest section, where they are only ≈50nm thick. Despite such an extreme geometry, these fibres were found to have good mechanical properties and tolerance to bending, and could be spliced to HNL standard fibre with splicing losses in accordance with the value expected from mode-field diameter mismatch.

The biggest challenge in the fabrication of HFs with sub-wavelength core dimension is to obtain a low transmission loss. There are three main loss mechanisms affecting small core HFs: confinement loss (which is due to the finite extent of the cladding region); absorption induced by surface and bulk hydroxyl impurity; and scattering loss due to surface roughness at the silica/air interfaces. For our fibre design, in which a large mode overlap was targeted, the latter two mechanisms are expected to be predominant, and must be addressed through careful fabrication procedures. The core and microstructured region were obtained from a single, very high purity silica rod produced by VAD. After ultrasonic drilling, the bores were mechanically polished, in order to reduce the surface roughness. Finally, the preform was dehydrated, using a standard technique, and fire polished.

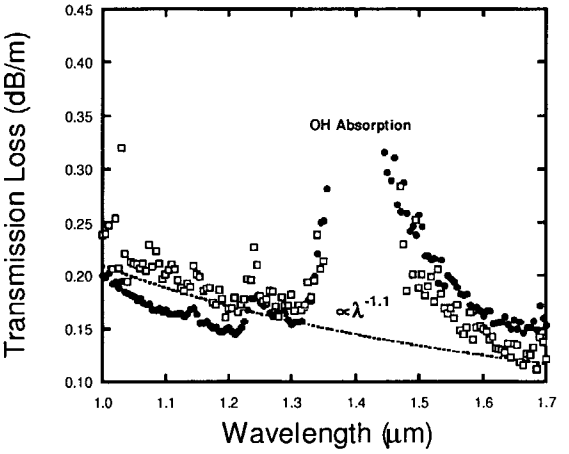

Figure 4: Loss spectra of two samples of SC-HF.

The transmission loss of the SC-HF was measured at 1.55μm, using a standard telecom laser source, as well as with a white light source. In the latter case, the SC-HF was spliced to a commercial HNL-HF, in order to improve the launch efficiency and avoid cladding modes. Fibre lengths of 100-200m were measured, and the results are shown in figure 4. The loss values of various samples range between 0.15-0.20 dB/m, and show only weak dependence on the wavelength (as opposed to the usual $\propto\lambda^{-4}$ dependence due to Rayleigh scattering). This is in good agreement with recent results by Roberts et al.[58] and is close to the inherent loss limit of surface roughness scattering due to frozen-in surface capillary waves. The loss spectrum also shows a strong absorption in the region 1350-1480nm. This is most probably due to surface hydroxyl (silanol) groups, which are known to cause attenuation values of several dB/m even in a partially saturated surface[59].

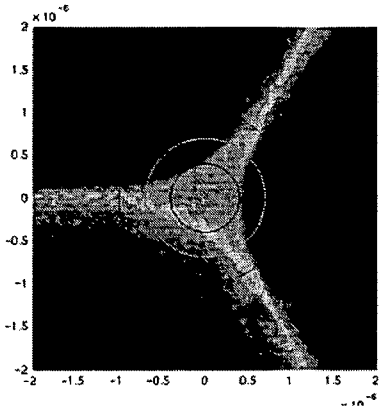

Figure 5: SEM image of the core of a SC-HF. Units are expressed in μm. The core diameter (blue line) is 0.8μm; 1.4 and 2μm diameter circles are also shown as a reference.

3.3. Theoretical analysis of transmission properties

The transmission properties of the SC-HF were modelled using a finite element method. The calculations were based on high magnification digitized SEM images (figure 5), in order to obtain more realistic predictions. The method used allows determination of the guided modes and their properties. These include the effective mode area, percentage of power in air and the confinement loss for different SC-HF structures. In particular, the dependence on the core diameter was studied simply by rescaling the whole structure. Figure 6 shows the modes (2dB contour plots) calculated at 1.55μm for four different core sizes (0.6, 0.8, 1 and 1.2 μm). It is obvious that the mode overlap with air increases with decreasing core size. The optical field distributions are not too dissimilar, but the mode becomes much less confined when d^{core}=0.6μm. The wavelength dependence of the effective mode area and fraction of power in air, calculated for different values of the core diameter, are shown in figure 7. The graphs very clearly show the same trend indicated by the mode profiles, i.e. the fraction of power in air increases with increasing λ and decreasing d^{core}. Correspondingly, the effective mode area decreases with decreasing d^{core}, however up to a certain point: for longer wavelengths the trend reverses. This is an indication of the mode becoming less and less confined to the core; correspondingly, the confinement loss was found to increase. Notice that, for the fibre with d^{core}=0.8μm, the confinement loss is negligible (less than 10^{-6}dB/m) in the wavelength range 0.4-1.8μm considered here.

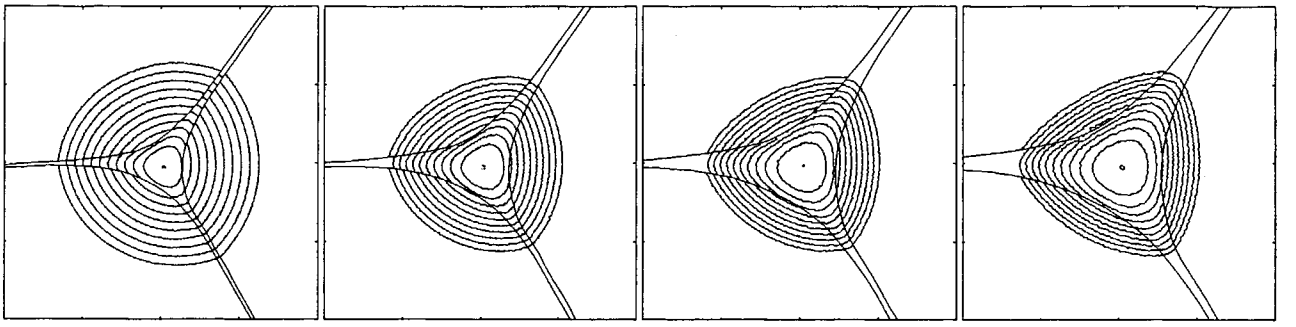

Figure 6: Calculated mode profiles at 1.55μm (2dB contour plots) of SC-HF structures with 0.6, 0.8, 1 and 1.2μm core diameters.

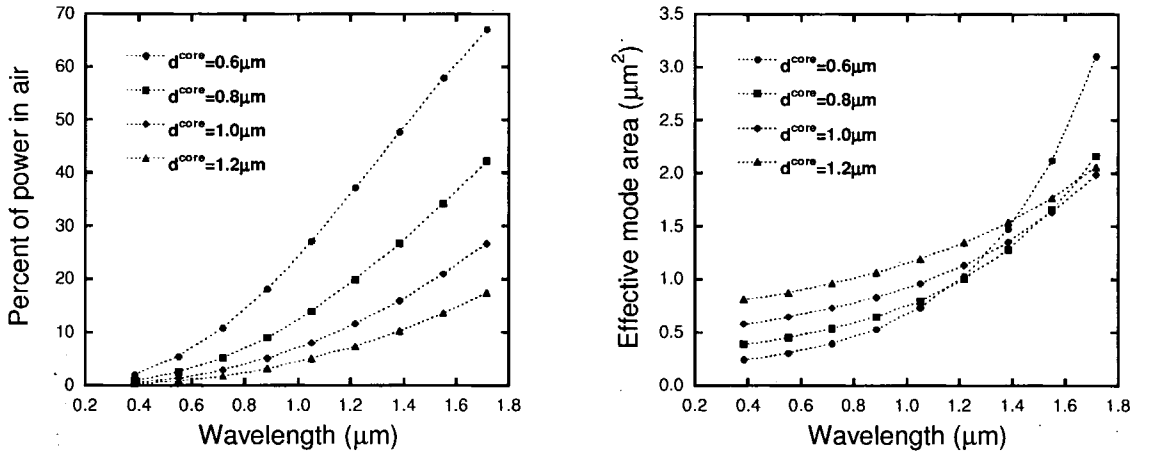

Figure 7: Calculated fraction of power in the holes (left) and effective mode area (right) of SC-HFs for different core diameters.

3.4. Evaluation of the SC-HF as an evanescent field sensor

We report some preliminary results on the performance of a SC-HF as an evanescent field device. The fibre was filled (from one end) with acetylene (ethyne, C_2H_2) at atmospheric pressure and room temperature, whilst monitoring the absorption in the 1.53μm region using an erbium-doped fibre ASE source and an optical spectrum analyzer with 10pm nominal resolution. Clearly, the biggest challenge with this type of structure is to achieve an efficient and stable launch condition. Free-space launch gave unsatisfactory long-term stability, therefore we spliced the SC-HF to a HNL standard fibre, which also prevented degradation of the end-faces of the HF due to water and dust contamination. Splice loss was however high at ≈10dB. Figure 8 shows the absorption of the P_{10} line ($\nu_1+\nu_3$ branch) of acetylene at 1530.98nm measured in a 0.625m long sample of SC-HF (0.8μm core). By comparing the absorption strength of the same line of acetylene using a standard free-path cell, we calculated a mode overlap of approximately 21.5%.

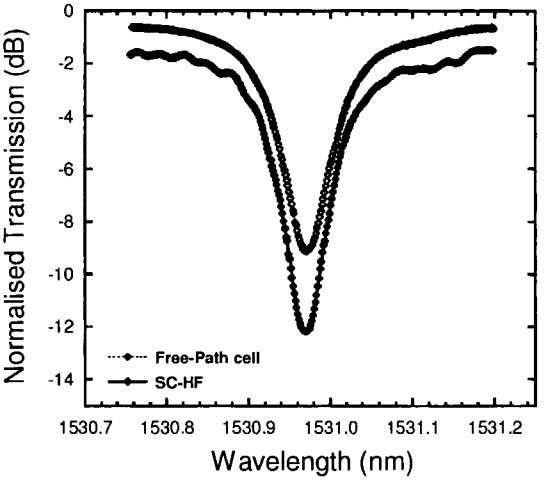

Figure 8: Normalised absorption of C_2H_2 at 1530.98nm in a 0.625m long SC-HF sample and in a 0.1m long free-path cell.

We believe that this value is to be regarded as a lower bound value, limited by the un-optimised launch conditions. However, this is the highest mode overlap factor ever reported in an index-guiding HF, almost twice as high as the value previously reported by Hoo, et al.,[56] and clearly shows the potential of the SC-HF for evanescent field sensing.

4. PHOTONIC BANDGAP FIBRES FOR USE AS GAS SENSORS

4.1. PBGFs for gas sensing

In photonic bandgap fibres, close to 100% mode overlap with air can be achieved by virtue of the optical field being tightly confined in the hollow core. In addition, hollow core PBGFs have two key properties that are advantageous for building compact and highly efficient sensors. The first advantage is the low bending loss, which allows them to be arranged in tight coils with no penalty in terms of the transmitted power. Secondly, PBGFs can be efficiently interfaced to conventional fibres. PBGFs operating in the 1.55μm window have approximately the same effective mode area as standard single-mode fibres, and can be spliced to conventional fibres with losses of 1-2dBs[60], although the conditions need to be right in order to preserve the structure in the vicinity of the splice. Achieving high mode overlap and low coupling losses results in a high sensitivity, which is highly desirable for the detection of weakly absorbing species or when using more cost-effective sources (e.g. LEDs)[61].

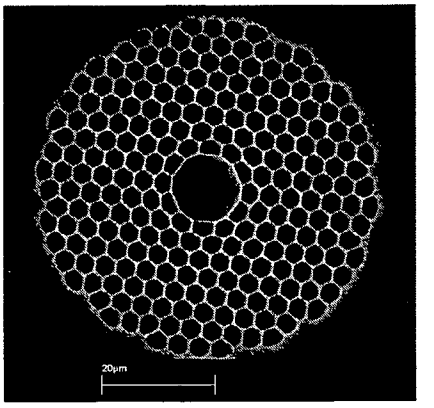

Figure 9: SEM micrograph of the PBGF used for the sensing experiment

As well as advantages, PBGFs have also a number of issues that may limit their practicality. Fibre loss, though generally low, is still usually greater than conventional fibres. Furthermore, long path lengths have the severe drawback of leading to long filling times. The very large surface/volume ratio present in PBGFs might induce chemical reactions with the fibre's walls. Lastly, the fibre ends of PBGFs are susceptible to contamination from water and dust particles and thus require adequate protection. Some of these aspects will be discussed in more detail in the next section.

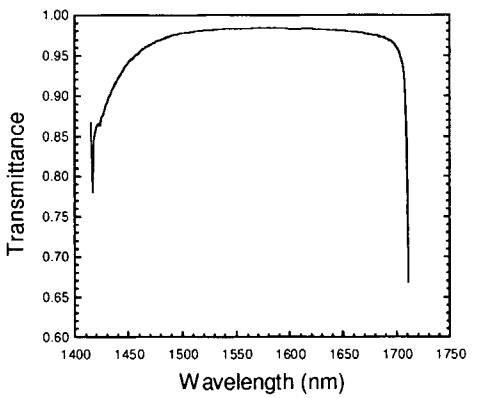

Figure 10: Transmission of the PBGF used in this study (1m length)

4.2. Absorption measurements of acetylene

We have evaluated the performance of a bandgap fibre as a gas sensor. Again, acetylene gas was employed due to the strong absorption lines located in the 1.55μm region. The PBGF used for the experiments was fabricated in-house and is shown in figure 9. It has a 7-point core defect, with a cladding composed of seven complete rings plus one further incomplete ring and. The fibre had a hole-to-hole spacing, Λ, of 3.6μm, a d/Λ ratio of 0.95 and an air filling factor ≈87%; the core diameter is 11.6μm. The bandgap is centered at approximately 1.57μm and the transmission loss, measured with a white light source, is 70dB/km; the transmission over 1m of fibre is shown in figure 10. Although PBGFs can by their very nature only transmit over a limited waveband, their transmission window (in this case, ≈200nm) is wide enough to overlap many absorption lines.

Previous work on gas sensing using MOFs employed bulky vacuum chambers[56,61]. In our effort towards a more practical system, we used miniaturized, gas-tight interfaces into which each fibre end was inserted. These interfaces have glass windows to allow an easy free-space launch into the fibre, and can be placed on standard micropositioners for accurate and repeatable alignment. Each cell has two inlets, allowing it to be readily filled with gas and/or evacuated. We also found that using such interfaces significantly reduces the possibility of contamination from water and dust, thereby

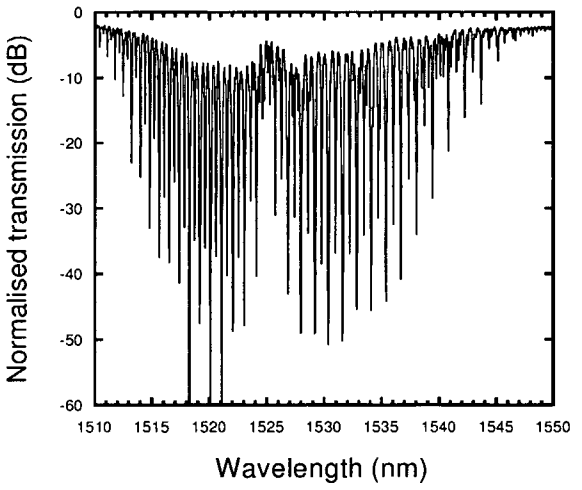

Figure 11: P- and R- braches of acetylene, measured in a 0.79m long PBGF sample

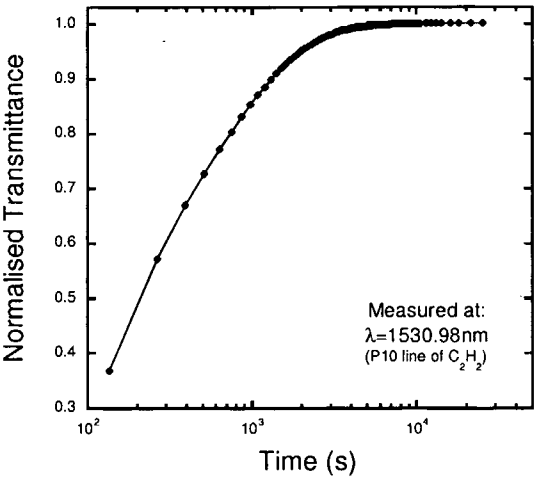

Figure 12: Dynamic of out-diffusion of acetylene from a 0.79m long PBGF sample

greatly extending the lifetime of the cleaved fibre endfaces relative to the case when they are left exposed to the atmosphere.

Absorption of acetylene was monitored by measuring the fibre transmission; to this purpose, we used an Er^{3+}-ASE source and an OSA. All measurements were taken at atmospheric pressure and at a temperature of 295K. Figure 11 shows the absorption spectrum of acetylene over a 0.79m length of PBGF, collected with a 0.05nm nominal resolution; both the P- and R- branches of the $\nu_1+\nu_3$ band are visible. Notice that the strongest lines are saturating, despite the large ≈55dB dynamic ratio.

We measured the characteristic time of free in- and out-diffusion of acetylene into the PBGF: the interfaces at each fibre end were filled with acetylene or left open to atmosphere, respectively. The volume of gas contained in each interface was much larger than the volume in the fibre holes. A typical result for the out-diffusion is shown in figure 12. The minimum transmittance at the wavelength corresponding to the P_{10} absorption line of acetylene (1530.98nm) was measured as a function of time. The characteristic time for a 0.79m length was ≈500s. The absorption line was still visible after ≈22hrs, giving a loss of approximately 2dB.

It is clear that the performance of a sensor based on a PBGF would be severely limited by the time necessary for the gas to diffuse in the holes. If a fast response time is required, a short length of fibre must be employed, thus reducing the sensitivity. In this instance, the advantage over conventional free-path cells would be less evident. Long path lengths and high sensitivity detection would only be feasible when a fast response time is not required and monitoring can take place over long time intervals. Some authors have proposed to introduce periodic openings along the fibre length in order to speed up the diffusion[56]; this, however, might prove very challenging in the case of a bandgap fibre and might also introduce significant loss, given that the guiding mechanism relies on the high regularity of cladding.

Recently, a much more practical use for these fibres has been demonstrated[60], where PBGFs are filled with gas and then permanently sealed. The absorption lines of the gas contained can be used as a fixed optical wavelength reference. Very stable gas cells can even be obtained by splicing a length of PBGF to conventional single mode fibre[60]. This solution allows obtaining long path lengths without the drawback of long filling time. We have investigated the use of PBGF gas cells in a practical gas sensor system and this application will be discussed in detail at the conference.

5. PHOTONIC BANDGAP FIBRES FOR MID-IR TRANSMISSION

5.1. Introduction

In PBGFs, light can be guided in a hollow core as a consequence of the bandgap effect, allowing for very weak interaction of the guided mode with the fibre structure. The possibility of obtaining silica-based fibres operating at wavelengths substantially beyond those feasible for conventional silica fibres is of course very intriguing and could find immediate applications in a wide range of areas, from power delivery to remote chemical and biological sensing and to military applications (such as targeting and threat detection). It is especially interesting for chemical sensing, since most of the strongest absorption lines occur beyond 2μm. Previous studies[28] have demonstrated the feasibility of air-guiding bandgap fibres based on materials that are not transparent at the operating wavelength, provided the cladding structure is designed to minimize the interaction with the guided mode. The typical loss values reported (≈1dB/m) are compatible with applications in optical sensing. Here we investigate bandgap fibre technology for beam delivery at other wavelengths of interest for remote sensing applications, specifically in the mid-IR region. The following sections are concerned with the design, fabrication and basic characterisation of PBGFs operating at wavelengths beyond 2μm.

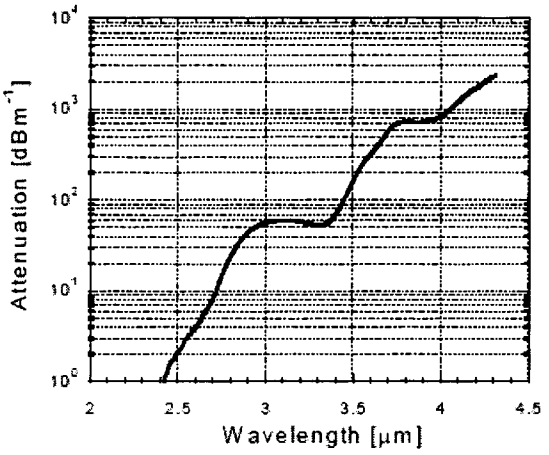

Figure 13: Spectral attenuation of dry synthetic silica (Heraeus Suprasil F300); taken from ref. 62

5.2. Design of mid-IR PBG Fibres

The transmission of standard silica fibres is limited to the near-IR for many practical purposes, due to the high material loss of silica beyond 2μm. In PBGFs, however, the light is almost entirely localised in the hollow core. If suitable structures could be identified where the overlap between the guided mode and the solid silica regions is sufficiently low, transmission at longer wavelengths, and possibly into the mid-IR, should in principle be possible even in the presence of high material loss. The optical attenuation of silica in the wavelength region beyond 2μm is determined by fundamental vibrational absorption, and by OH absorption[62]. This makes low-OH grade silica (such as Suprasil F300 from Heraeus) the material of choice for PBGFs designed for mid-IR transmission. As seen in fig. 13, the loss increase is approximately exponential with increasing wavelength, as expected for the "multiphonon edge"[63]. We identified the region between 2.9 and 3.45μm as the ideal target for the present study; here silica loss is not prohibitively high (of the order of 50dBm^{-1}) and only weakly dependent on wavelength.

Due to their structural complexity, design is a paramount aspect of PBGF technology. As pointed out before, the fibre properties (including position of the bandgap, bandwidth and transmission loss) are strongly dependent on the fine details of the fibre structure[41]. Again, we employed a finite element method to calculate the transmission properties of realistic PBGF structures. As far as modeling is concerned, the main difference between PBGFs operating in the mid-IR and near-IR is that material effects have a much larger impact on the properties of the former. Silica loss is very low in the near-IR, therefore it is generally omitted from the models without affecting the accuracy of their predictions.

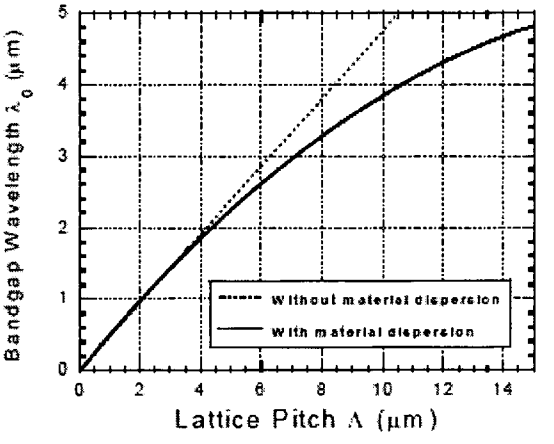

Figure 14: Central wavelength of the bandgap vs lattice pitch Λ with and without accounting for the dispersion of silica (d/Λ=0.95, AFF=90%).

This is not the case for mid-IR wavelengths, where material loss needs to be included in the calculations and its effect carefully evaluated. Besides the loss, the material dispersion also needs to be taken into account. For near-IR fibres a fixed value of refractive index is generally assumed, leading to the following scaling law:

(1) $\lambda_0/\Lambda \approx$ constant

where λ_0 is the central wavelength of the bandgap, Λ is the lattice pitch, and the value of the constant depends on the air filling factor and on the hole shape. Due to material dispersion, however, if the simple scaling law (1) was applied to obtain the design of a mid-IR structure from a near-IR operating fibre, large errors would result. Fig. 14 shows the calculated λ_0 vs Λ dependence for a PBGF structure with $d/\Lambda=0.95$ and an air filling factor of 90%, with and without accounting for the material dispersion; the two curves differ significantly for $\lambda_0>2\mu m$. When the material dispersion is included in the model, a lattice pitch from 6.5 to 7.5μm is found to correspond to an operating wavelength of 3μm, depending on the value of d/Λ and of the air filling factor.

5.3. Theoretical analysis

We performed a theoretical study of the effect of the material loss, using the finite-element method, on a fibre designed for operation around 3μm. The fibre considered here had a pitch of 6.5μm, a d/Λ of 0.94 and an air filling factor of approximately 88%. The predicted fibre loss is shown in fig. 15. The dashed trace is the pure confinement loss of the fibre, showing that the structure supports a bandgap centered at approximately 2.95μm. The continuous trace is the fibre loss obtained by including a material loss of 50dB/m in the calculation. The result clearly indicates that the bandgap is preserved, and the predicted fibre loss (contributions due to confinement and absorption only) is of the order of $1dBm^{-1}$.

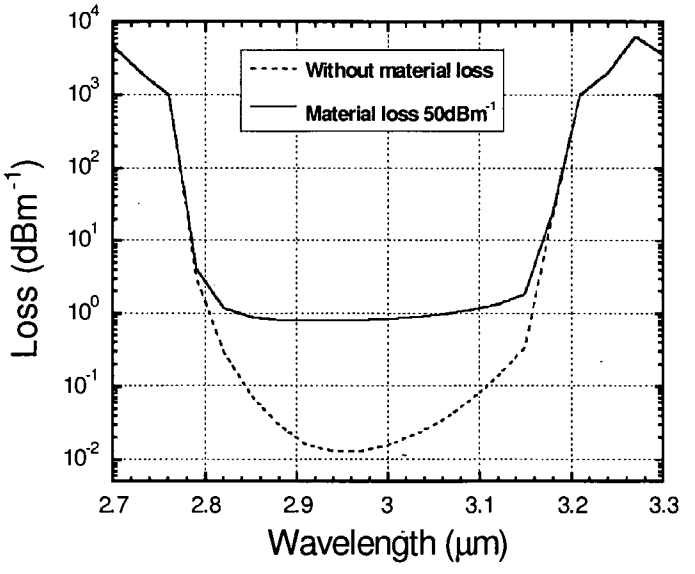

Figure 15. Calculated fibre confinement loss with and without accounting for the material loss of ®Suprasil F300 (50dB/m @3μm), showing the bandgap is preserved.

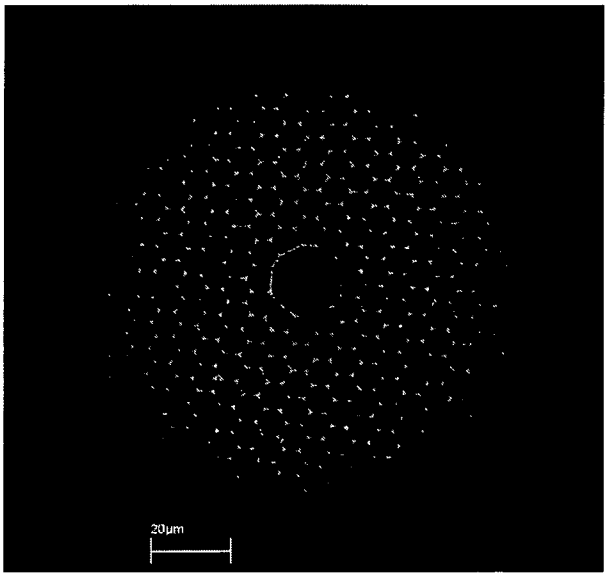

Figure 16: SEM micrograph of an air/silica PBGF designed for long wavelength operation

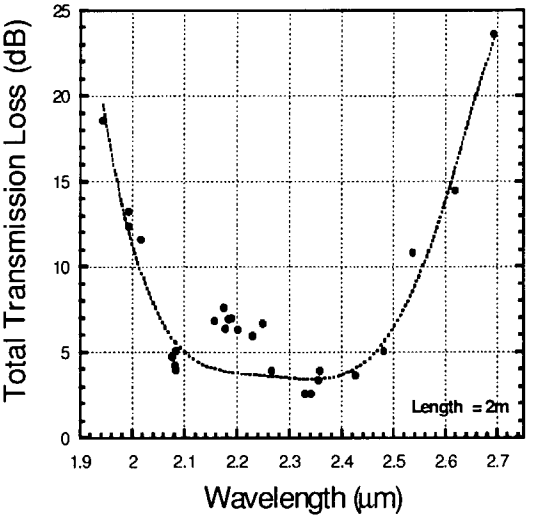

Figure 17: Transmission over 2m length.

5.4. Fabrication of PBGF for long wavelength transmission

Figure 16 shows a bandgap fibre designed for transmission beyond 2µm. The fibre has a lattice pitch, Λ, of 6.45µm, i.e. a similar value assumed in our theoretical study. The fibre has a seven point core defect surrounded by seven complete rings (plus one further incomplete ring) having excellent geometry. The hollow region (comprising core and cladding) measures about 110µm across, while the fibre diameter is 340µm. This value of fibre OD is probably as close to the maximum that is practical for applications in which the fibre needs to be bent or coiled. It is clear that the constraint on the fibre OD will ultimately pose a limit on the maximum number of rings of holes that can be obtained in a practical structure, which impacts on the mode confinement and ultimately on the fibre loss. As seen from the graph in figure 14, this factor becomes more and more limiting as longer operating wavelengths are targeted. Due to the large expansion imposed on the structure during fabrication, in order to achieve the large value of pitch, the d/Λ and air filling factor are larger than the values used for the calculations. This results in a substantial shift of the central wavelength of the bandgap towards shorter wavelengths.

The fibre transmission was measured using an OPO source. The output could be tuned in the range 2-3.5µm. Figure 17 shows the spectral transmission (normalized to the input power) of a 2m long sample of PBGF. The bandgap extends from 2 to 2.6µm, with maximum transmission at 2.35mm. A region of relatively higher loss is located at about 2.2µm, and is probably due to absorption from surface hydroxyl (silanol) impurity[62]; if this is the case, it is possible that the long-wavelength edge in the transmission spectrum is due to the fundamental OH vibration at ≈2.7µm. Another possible loss mechanism is anticrossing with surface modes[44], although the calculations did not show evidence of such modes in our structures. The transmission loss was measured by the cutback method, yielding a value of 0.8dB/m at the central wavelength 2.35µm.

6. CONCLUSIONS

In this work, we have discussed the key properties of air/silica microstructured fibres for sensor applications. Both index-guiding holey fibres and photonic bandgap fibres have attractive qualities for chemical sensing. By careful design of their structure, index-guiding holey fibres can be achieved with very large mode field overlap with the air holes, which can be exploited for evanescent field devices. Photonic Bandgap fibres, where the mode is almost entirely guided

in the central hollow core, also have great potential for chemical sensing and, in view of the ease of splicing to conventional fibres, can also be used to fabricate compact sealed gas cell units for use as fixed reference cells. The very low overlap with the silica structure in hollow-core PBGFs can be exploited in order to extend the operational range of silica-based fibres to wavelength beyond 2μm.

ACKNOWLEDGEMENTS

The authors acknowledge the support of an OSDA DTI Link grant (PFIDEL): EPSRC grant number GR/SO5793-01 and also support from the Electro-Magnetic Remote Sensing (EMRS) Defence Technology Centre, established by the UK Ministry of Defence. The authors also acknowledge A.S. Webb and J.K. Sahu for useful discussion on the preparation of the SC-HF preform. The VAD perform used for the SC-HF was supplied by Furukawa Electric Co. Ltd, Japan.

REFERENCES

1. J.C. Knight, T.A. Birks, P.St.J.Russell, D.M. Atkins, "All-silica single-mode optical fiber with a photonic crystal cladding", Opt Lett, **21,** pp.1547-1549 1996.
2 J. Broeng, D. Mogilevstev, S.E. Barkou, A. Bjarklev, "Photonic crystal fibers: A new class of optical waveguides,"Opt. Fiber Tech. **5** (1999) 305.
3 T.M. Monro, D.J. Richardson "Holey optical fibres: fundamental properties and device applications", C.R. Phys. **4,** pp. 175-186, (2003).
4 P.St.J. Russell, "Photonic crystal fibers," Science **299**, pp. 358 - 362, 2003.
5 J.C. Knight, "Photonic crystal fibres," Nature **424**, pp. 847 - 851, 2003.
6 T.M. Monro, Y.D. West, D.W. Hewak, N.G.R. Broderick, D.J. Richardson, "Chalcogenide holey fibers", Electron. Lett., **36**, 1998-2000, 2000.
7 K.M. Kiang, K. Frampton, T.M. Monro, R. Moore, J. Tucknott, D.W. Hewak, D.J. Richardson, H.N. Rutt, "Extruded single-mode nonsilica glass holey optical fibres", Electronics Letters, **38**, .546-547, 2002.
8 V.V.R Kumar, A.K George, J.C.Knight, P.St.J. Russell, "Tellurite photonic crystal fibre", Opt. Express, **11**, 2641-2645, 2003.
9 H. Ebendorff-Heidepriem, P. Petropoulos, S. Asimakis, V. Finazzi, R.C. Moore, K. Frampton, F. Koizumi, D.J. Richardson, T.M. Monro, "Bismuth glass holey fibers with high nonlinearity", Optics Express, **12**, 5082-5087, 2004.
10 M.A. van Eijkelenborg, M.C.J. Large, A. Argyros, J. Zagari, S. Manos, N.A. Issa, I. Bassett, S. Fleming, R.C. McPhedran, C.M. de Sterke , N.A.P. Nicorovici, "Microstructured polymer optical fiber", Opt. Express, **9**, 319-327, 2001.
11 E. Rave, P. Ephrat, M. Goldberg, E. Kedmi, A. Katzir, "Silver halide photonic crystal fibers for the middle infrared", Appl. Opt., **43**(11), 2236-2241, 2004.
12 T.M. Monro, P.J. Bennett, N.G.R. Broderick, D.J. Richardson, "Holey fibers with random cladding distributions," Opt. Lett., **25**, 206-208 (2000).
13 J.C. Knight, J. Broeng, T.A. Birks, and P.St.J. Russell, "Photonic bandgap guidance in optical fibers," Science, **282**, 1476-1478 (1998).
14 S.M. Maughan, H.H. Kee, T.P. Newson, "Simultaneous distributed fibre temperature and strain sensor using microwave coherent detection of spontaneous Brillouin backscatter", Meas. Sci. Technol., **12**(7), 834-842 (2001).
15 F.T.S. Yu, S. Yin (Eds.), "Fiber Optic Sensors", Dekker, New York, 2002.
16 Byoungho Lee, "Review of the present status of optical fiber sensors", Opt. Fiber Tech. **9,** 57-79 (2003).
17 A. Othonos, K. Kalli, "Fiber Bragg Gratings-Fundamentals and Applications in Telecommunications and Sensing", Artech House, Boston, 1999.
18 J. Blake, "Fiber optic gyroscopes", in: K.T.V. Grattan, B.T. Meggitt (Eds.), Optical Fiber Technology, Vol. 2, Chapman and Hall, New York, 1998, pp. 303–328.
19 P.B. Ruffin, "Fiber gyroscope sensors", in: F.T.S. Yu, S. Yin (Eds.), Fiber Optic Sensors, Dekker, New York, 2002, pp. 383–415.

20 G.D. Peng, P.L. Chu, "Optical fiber hydrophone systems", in: F.T.S. Yu, S. Yin (Eds.), Fiber Optic Sensors, Dekker, New York, 2002, Chap. 9, pp. 417–447.

21 T.M. Monro, W. Belardi, K. Furusawa, N.G.R. Broderick, D.J. Richardson, "Microstructured optical fibers: new opportunities for sensing", OFS 2000 Venice, 2000, paper Fr4-2.

22 T.M. Monro, W. Belardi, K. Furusawa, J.C. Baggett, N.G.R. Broderick, D.J. Richardson "Sensing with microstructured optical fibers" Meas. Sci. Technol. **12,** 854-858 (2001).

23 J.H. Rothwell, D.H. Flavin, W.N. MacPherson, J.D.C. Jones, J.C. Knight, P.St.J. Russell, "Photonic sensing based on modulation of propagation properties of photonic crystal fibres", Proc. SPIE Vol. 5855, 122-125 (2005).

24 P.M. Blanchard, J.G. Burnett, G.R.G. Erry, A.H. Greenway, P. Harrison, B. Mangan, J.C. Knight, P.St.J. Russell, M.J. Gander, R. McBride, J.D.C. Jones "Two-dimensional bend sensing with a single, multicore optical fibre", Smart Mater. Struct. **9**, 132-140 (2000)

25 W.N. MacPherson, E.J. Rigg, J.D.C. Jones, V.V. Ravi Kanth Kumar, J.C. Knight, P.St.J. Russell, "Finite-element analysis and experimental results for a microstructured fibre with enhanced hydrostatic pressure sensitivity", J. Lightwave Technol., **23**, 1227-1331 (2005).

26 P. Petropoulos, F. Poletti, J.Y.Y. Leong, T.M. Monro, H. Ebendorff-Heidepriem, V. Finazzi, V. Tse, X. Feng, S. Asimakis, N.G. Broderick, D.J. Richardson, "High nonlinearity holey fibers: design fabrication and applications", CLEO/IQEC-Pacific Rim, Tokyo, 2005.

27 B. Povazay, K. Bizheva, A. Unterhuber, B. Hermann, H. Sattmann, A. F. Fercher, and W. Drexler, A. Apolonski W. J. Wadsworth, J. C. Knight, and P. St. J. Russell, M. Vetterlein and E. Scherzer, "Submicrometer axial resolution optical coherence tomography", Opt. Lett., **27**(20), 1800-1802 (2002).

28 B. Temelkuran, S.D. Hart, G. Benoit, J.D. Joannopoulos, Y. Fink, "Wavelength-scalable hollow optical fibres with large photonic bandgaps for CO_2 laser transmission", Nature, **420**, 650-653 (2002).

29 S.E. Barkou, J. Broeng, A. Bjarklev, "Silica–air photonic crystal fiber design that permits waveguiding by a true photonic bandgap effect", Opt. Lett. 24(1), 46-48, (1999)

30 N.A. Mortensen, M.D. Nielsen, J. R. Folkenberg, C. Jakobsen, H.R. Simonsen, "Photonic crystal fiber with a hybrid honeycomb cladding", Opt. Expr. **13**(3), 468-472 (2004)

31 N.A. Mortensen, M.D. Nielsen, "Modeling realistic cladding structures for air-core photonic bandgap fibres", Opt. Lett. **29**(4), 349-351 (2004)

32 T.M. Monro, A.Bjarklev, J. Laegsgaard, "Microstructured optical fibres", in Handbook of Optoelectronics, J.P. Dakin and R.Brown, eds., IOP, Bristol, 2005.

33 K. Tajima, J. Zhou, K. Kurokawa, K. Nakajima, "Low water peak photonic crystal fibres", Proc. ECOC '03, Rimini, 2003, 42-43

34 A. Mori, K. Shikano, K. Enbutsu, K. Oikawa, K. Nagamura, M. Kato, S. Aozasa, "1.5mm band zero-dispersion shifted tellurite photonic crystal fibre with a nonlinear coefficient of $675W^{-1}km^{-1}$", ECOC 2004, Stockholm, 2004, paper Th3.3.6.

35 K.M. Kiang, K. Frampton, T.M. Monro, R. Moore, J. Tucknott, D.W. Hewak, D.J. Richardson, H.N. Rutt," Extruded single-mode nonsilica glass holey optical fibres", Electronics Letters, **38**, .546-547, (2002).

36 R. Bise, D.J. Trevor, "Sol-gel derived microstructured fiber: fabrication and characterisation", OFC 2005, Anheim, paper OWL6.

37 T.M. Monro, P.J. Bennet, N.G.R. Broderick, D.J. Richardson, "Holey fibres with random cladding distributions", Opt. Lett. **25**, 206-208, (2000)

38 D. Kominsky, G.R. Pickrell, R.H. Stolen, "Genaration of random-hole optical fibres", Opt. Lett. **28**(16), 1409-1411, (2003)

39 J.C. Knight, J. Broeng, T.A. Birks, P.St.J. Russell, "Photonic bandgap guidance in optical fibres", Science, **282**, 1476-1478 (1998).

40 T.A. Birks, P.J. Roberts, P.St.J. Russell, D.M. Atkin and T.J. Shepherd, "Full 2-D photonic bandgap in silica/air structures", Electon. Lett. **31**(22), 1941-1943 (1995).

41 K.Saitoh, M. Koshiba, "Leakage loss and group velocity dispersion in air-core photonic bandgap fibers" **11**(23), 3100-3109 (2003).

42 L. Brandon Shaw, J.S. Sanghera, I.D. Aggarwal, F.H. Kung, "As-S and As-Se based photonic band gap fiber for IR laser transmission", Opt. Expr. **11**(25), 3455-3460 (2003)

43 C.M. Smith, N. Venkataraman, M.T. Gallagher, D. Müller, J.A. West, N.F. borrelli, D.C. Allan, K.W. Koch, "Low-loss hollow-core silica/air photonic bandgap fibre", Nature **424**, 657-659 (2003).

44 J.A. West, C.M. Smith, N.F. Borrelli, D.C. Allan, K.W. Koch, "Surface modes in air-core photonic bandgap fibres" Opt. Expr. **12**(8), 1485-1496 (2004).

45 B.J. Mangan, L. Farr, A. Langford, P.J. Roberts, D.P. Williams, F. Couny, M. Lawman, M. Mason, S. Coupland, R. Flea, H. Sabert, T.A. Birks, J.C. Knight, P.J.St. Russell, , Proc. OFC 2004, paper PDP24.

46 L. Michaille, D.M. Taylor, C.R. Bennett, T.J. Shepard, C. Jacobsen, T.P. Hansen, "Damage threshold and bending properties of photonic crystal and photonic bandgap fibres", Proc. SPIE, vol. 5618, 30-38 (2004)

47 D.G. Ouzounov, F.R. Ahmad, D. Müller, N. Venkataraman, M.T Gallagher, M.G. Thomas, J. Silcox, K.W. Koch, A.L. Gaeta, "Generation of megawatt optical solitons in hollow-core photonic band-gap fibers", Science **301**,1702-1704 (2002)

48 F. Benabid, J.C. Knight, G. Antonopoulos, P.St.J. Russell, "Stimulated Raman Scattering in Hydrogen-Filled Hollow-Core Photonic Crystal Fiber",Science **298**, 399-402 (2002)

49 F. Benabid, J.C. Knight, P.St.J. Russell, "Particle levitation and guidance in hollow-core photonic crystal fiber", Opt. Expr.**10**, 1195-1203 (2002).

50 S.G. Johnson, M. Ibanescu, M. Skorobogatiy, O. Weisberg, T.D. Engeness, M. Soljacic, S.A. Jacobs, J.D. Joannopoulos, Y. Fink, "Low-loss asymptotically single-mode propagation in large-core OmniGuide fibers" Opt. Expr. **9**, 748-779 (2001)

51 G. Vienne , Y. Xu, C. Jacobsen, H.J. Deyerl, J.B. Jensen, T.Sorensen, T.P Hansen, Y. Huang, M.Terrel, R.K. Lee, N.A. Mortensen, J. Broeng, H. Simonsen, A. Bjarklev, A. Yariv, "Ultra-large bandwidth hollow-core guiding in all-silica Bragg fibers with nano-supports" Opt. Expr **12**(15), 3500-3508, 2004.

52 T.M. Monro, D.J. Richardson, P.J. Bennett, "Developing holey fibres for evanescent field devices", Electron. Lett. **35**, 1188-1189 (1999).

53 G. Stewart, F.A. Muhammad, B. Culshaw, "Sensitivity improvement for evanescent-wave gas sensors" Sens. Actuators B **11**, 521-524 (1993)

54 T.M. Monro, W. Belardi, K. Furusawa, J.C. Baggett, N.G.R. Broderick, D.J. Richardson "Sensing with microstructured optical fibers" Meas. Sci. Technol. **12,** 854-858 (2001).

55 Y.L. Hoo, W. Jin, H.L. Ho, D.N. Wang, R.S. Windeler, "Evanescent gas sensing using microstructure fiber", Opt. Eng. **41**(1), 8-9 (2002).

56 Y.L. Hoo, W. Jin, C. Shi, H.L. Ho, D.N. Wang, S.C. Ruan, "Design and modeling of a photonic crystal fiber gas sensor" Appl. Opt. **42**(18), 3509-3515 (2003).

57 The result refers to Crystal Fibre's HNL-HF: d^{core}=1.7μm, Λ=3.24μm and d/Λ=0.925; see www.crystal-fibre.com

58 P.J. Roberts, F.Couny, H. Sabert, B.J. Mangan, T.A. Birks, J.C. Knight, P.St.J Russell, "Loss in solid-core photonic crystal fibres due to interface roughness scattering", Opt. Exp. **13**(20), 7779-7793 (2005)

59 R.T. Bise, D.J. Trevor, "Surface Absorption in Microstructured Optical Fibers", Proc. OFC 2004, paper WI4.

60 F. Benabid, F. Couny, J.C. Knight, T.A. Birks, P.St.J Russell, "Compact, stable and efficient all-fibre gas cells using hollow-core photonic crystal fibres", Nature, **434**, 488 - 491 (2005)

61 T. Ritari, J. Tuominen, H. Ludvigsen, J.C. Petersen, T. Sorensen, T.P. Hansen, H.R. Simonsen, "Gas sensing using air-guiding photonic bandgap fibers", Opt. Expr. **12**(17), 4080-4087 (2004)

62 O. Humbach, H. Fabian, U. Grzesik, U. Haken, W. Heitmann, "Analysis of OH absorption bands in synthetic silica", J. non-Cryst. Solids **203**, 19-26 (1996)

63 Bach, H. and Neuroth, N. (Eds.), "The properties of optical glass", 1995, Springer